Ultrafast Hydration Dynamics in the Lipidic Cubic Phase: Discrete Water Structures in Nanochannels

Jongjoo Kim,[†] Wenyun Lu,[†,§] Weihong Qiu,[†] Lijuan Wang,[†] Martin Caffrey,[‡] and Dongping Zhong*[,†]

Departments of Physics, Chemistry, and Biochemistry, Programs of Biophysics, Chemical Physics, and Biochemistry, The Ohio State University, Columbus, Ohio 43210, and Department of Chemical and Environmental Sciences, Materials and Surface Science Institute, University of Limerick, Limerick, Ireland

Received: May 8, 2006

We report here our studies of hydration dynamics of confined water in aqueous nanochannels (∼50 Å) of the lipidic cubic phase. By systematically anchoring the hydrocarbon tails of a series of tryptophan−alkyl ester probes into the lipid bilayer, we mapped out with femtosecond resolution the profile of water motions across the nanochannel. Three distinct time scales were observed, revealing discrete channel water structures. The interfacial water at the lipid surface is well-ordered, and the relaxation dynamics occurs in ∼100−150 ps. These dynamically rigid water molecules are crucial for global structural stability of lipid bilayers and for stabilization of anchored biomolecules in membranes. The adjacent water layers near the lipid interface are hydrogen-bonded networks and the dynamical relaxation takes 10−15 ps. This quasi-bound water motion, similar to the typical protein surface hydration relaxation, facilitates conformation flexibility for biological recognition and function. The water near the channel center is bulklike, and the dynamics is ultrafast in less than 1 ps. These water molecules freely transport biomolecules near the channel center. The corresponding orientational relaxation at these three typical locations is well correlated with the hydration dynamics and local dynamic rigidity. These results reveal unique water structures and dynamical motions in nanoconfinements, which is critical to the understanding of nanoscopic biological activities and nanomaterial properties.

I. Introduction

Water confined in self-organized molecular assemblies is of great interest to biology and materials.[1−10] Examples of water molecules in such restricted environments are abundant such as at surfaces[1,11,12] and in the interior of proteins,[13−15] in the grooves of DNA,[16,17] on micelles or in water pools of reverse micelles,[18−20] and in porous materials.[5,21,22] Elucidation of these confined water structures and dynamics is central to understanding biological functions and the material properties of their associated macromolecules. A variety of spectroscopic techniques[11,12,18,20,23−27] have been used to characterize these water structures. Very recently, a unique water structure with anomalously soft dynamics inside single-walled carbon nanotubes has been reported.[28] Here, we use a model system of water nanochannels formed in the lipidic cubic phase (*Pn*3*m*) and systematically examine water dynamics across the channel.

The lipidic cubic phase has recently been demonstrated as a new system in which to crystallize membrane proteins,[29,30] and several examples[29,31,32a] have been reported. The molecular mechanism for such crystallization is not yet clear, but the interfacial water and transport are believed to play an important role in nucleation and crystal growth.[32b,c] Through the use of a related model system of reverse micelles, drastic differences in water behavior were observed, both experimentally[2,18,20] and theoretically.[9,33] In contrast to the ultrafast motions of bulk water that occur in less than several picoseconds, significantly slower water dynamics were observed in hundreds of picoseconds, indicating a well-ordered water structure in these confinements.

In this study, we use an amphiphilic fluorescence probe tethered to lipid bilayers with a variable alkyl chain length. The chromophore is an indole moiety, and the probes are a series of tryptophan (Trp)−alkyl ester molecules. Presumably, the hydrophobic alkyl chains systematically anchor the chromophore to different depths of the lipid bilayer, enabling it to sample various aqueous environments and probe different layers of water dynamics, conceptually shown in Figure 1. We first studied the simplest system of a Trp-laced cubic phase. With femtosecond resolution, we observed three types of water dynamics with distinct time scales, indicating a distribution of bulklike, quasi-bound, and well-ordered water structures across the nanochannel. With changes in alkyl length, we set out to systematically examine these three discrete water structures. We also studied interactions of a 26 amino acid peptide, melittin,[34] with lipids in the cubic phase using a single intrinsic tryptophan (Trp19) as the probe.

The paper is organized as follows. In section II, we describe the experimental method including the femtosecond laser apparatus and sample preparation. In section III, we present the femtosecond-resolved experimental results and discussion on water dynamics and structures in the nanochannel. The conclusion of our work is summarized in section IV. In a related study, the interaction of tryptophan, tryptophan peptides, and tryptophan alkyl esters at the curved membrane interfaces of the cubic phase has been examined.[32d]

II. Experimental Section

A. Femtosecond Laser Setup. All the femtosecond-resolved measurements were carried out using a fluorescence up-

* Author to whom correspondence should be addressed. Phone: (614) 292-3044. Fax: (614) 292-7557. E-mail: dongping@mps.ohio-state.edu.
[†] The Ohio State University.
[‡] University of Limerick.
[§] Present address: Lewis−Sigler Institute for Integrative Genomics, Princeton University, Princeton, NJ 08544.

10.1021/jp062806c CCC: $33.50
Published on Web 10/11/2006

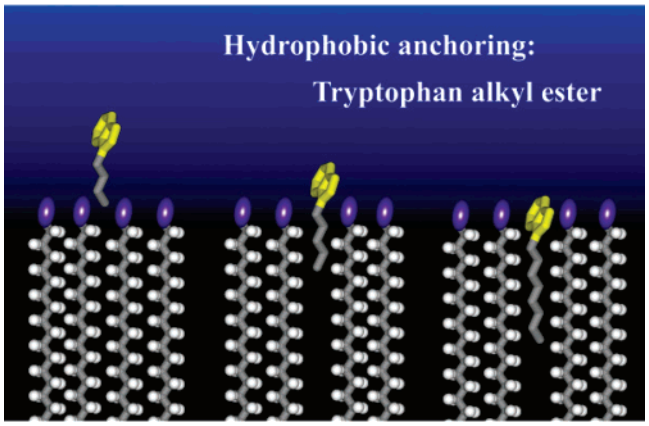

Figure 1. Schematic representation of the concept for probing different layers of water near lipid−water interfaces through anchoring hydrocarbon tails of a series of Trp−alkyl ester probes into lipids. The blue gradient represents different distributions of water structures, and the yellow ring is the indole chromophore.

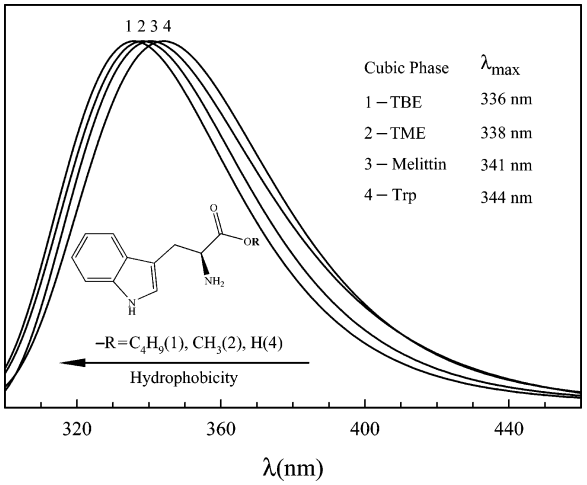

Figure 2. Normalized steady-state fluorescence emissions from four Trp probes: tryptophan, melittin, TME, and TBE. Note the correlation between emission maxima and their hydrophobicities.

conversion method. The integrated experimental setup has been described elsewhere.[35] Briefly, a 1 mJ femtosecond pulse, centered at 800 nm with a temporal width of 110 fs and a repetition rate of 1 kHz, was used to pump an optical parametric amplifier (OPA-800C, Spectra-Physics) to generate signal (1289 nm) and idler (2109 nm) beams. The latter was mixed with the residual fundamental (800 nm) in a 0.2-mm-thick β-barium borate crystal (BBO, type I) to generate a femtosecond pulse at 580 nm. This femtosecond pulse, compressed through a pair of prisms with double paths to reach a temporal resolution of 60 fs, was frequency-doubled to generate our pump wavelength at 290 nm by another 0.2-mm-thick BBO crystal. The pump pulse energy was typically attenuated to ~140 nJ prior to being focused into the motor-controlled moving sample cell. The fluorescence emission was collected by a pair of parabolic mirrors and mixed with a gating pulse (800 nm) in a 0.2-mm-thick BBO crystal through a noncollinear configuration. The up-converted signal ranging from 218 nm to 292 nm was detected by a photomultiplier coupled with a double-grating monochromator. The instrument response time under the current noncollinear geometry is between 400 and 500 fs as determined from the up-conversion signal of Raman scattering by water at approximately 320 nm.

The pump-beam polarization was set at the magic angle (54.7°) with respect to the acceptance axis (vertical) of the up-conversion crystal, and the polarization of the gating beam was set parallel to this axis through a half-wave plate. For fluorescence anisotropy measurements, the pump-beam polarization was rotated either parallel or perpendicular to the acceptance axis to obtain the parallel ($I_{||}$) and perpendicular signal ($I_{\perp}$), respectively. These transients were used to construct time-resolved anisotropy

$$r(t) = (I_{||} - I_{\perp})/(I_{||} + 2I_{\perp})$$

B. Sample Preparation. Monoolein (1-oleoyl-*rac*-glycerol, >99% purity) was purchased from Nu Chek Prep, Inc. (Elysian, MN). Tryptophan, hydrochloride salts of tryptophan methyl ester (TME), tryptophan ethyl ester (TEE), tryptophan butyl ester (TBE), and tryptophan octyl ester (TOE), and melittin in lyophilized powder were acquired from Sigma-Aldrich. All other chemicals were obtained from Fisher Scientific and used as received without further purification. The lipid−water mixture was made at 20 °C consisting of 63% (w/w) monoolein and 37% (w/w) aqueous solution containing 4 mM Trp−alkyl ester or 2 mM melittin and 25 mM Na/K phosphate buffer at pH 5.6. Under these conditions, the mixture forms the lipidic cubic phase (*Pn*3*m*) with an aqueous channel diameter of ~50 Å.[36]

C. Steady-State Fluorescence Characterization. The tryptophan fluorescence emission peaks at 349 nm in bulk water and shifts to 352 nm in 100 mM Tris buffer at pH 7.5. The steady-state fluorescence spectra of several typical Trp probes in the lipidic cubic phase recorded using a Spex FluoroMax-3 are shown in Figure 2. The emission of tryptophan in the water channel has a maximum at 344 nm, and the peak shifts to 341 nm for melittin, 338 nm for TME, 337 nm for TEE, and 336 nm for TBE and TOE. These emission peaks systematically shift to the blue, indicating that the hydrocarbon tail anchors the chromophore deeper and deeper in the lipid bilayer, consistent with the increase of hydrophobicity of their local environments. This observation with the hydration and anisotropy dynamics detailed below excludes the possibility that the observed gradual blue shift in emission is due to the enhanced distribution of the Trp probes into the lipid bilayer.[32b,c] The Trp probes are primarily located around lipidic interfaces. Here, we focus on femtosecond-resolved studies of tryptophan, melittin, TME, and TBE in the lipidic cubic phase (Figure 2).

III. Results and Discussion

A. Femtosecond-Resolved Fluorescence Dynamics. A series of typical femtosecond-resolved fluorescence up-conversion transients of Trp, melittin, TME, and TBE in the cubic phase is shown in Figures 3−5. More than 10 emission wavelengths of each Trp probe were gated from the blue to the red side of the emission peak. A global fitting strategy was used to fit all the transients. Typically, four or five exponential functions were used, and among these are two lifetime emission decays. The other two or three components result from solvation relaxation. The two fluorescence lifetimes (500 ps and 3 ns) were fixed for all transients.[12]

At the blue side of the emission maximum, all transients obtained from four Trp probes in the cubic phase aqueous channels drastically slow down compared to that of tryptophan in bulk water. The transients show significant solvation dynamics covering three orders of magnitude on time scales from subpicosecond to a hundred picoseconds. These solvation dynamics can be represented by three distinct decay components: The first component occurs in approximately 1 ps, the second decays in tens of picoseconds, and the third takes a hundred

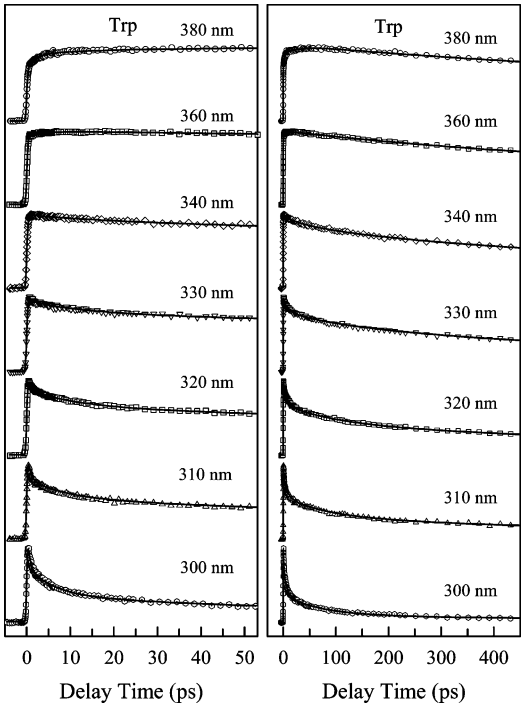

Figure 3. Normalized femtosecond-resolved fluorescence transients of tryptophan in the aqueous channels of the cubic phase in the short (left) and long (right) time ranges with a series of gated fluorescence emissions.

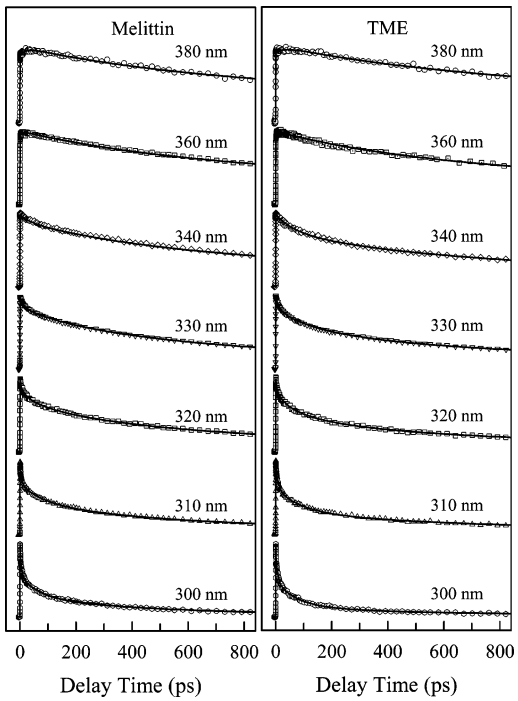

Figure 4. Normalized femtosecond-resolved fluorescence transients of membrane-bound α-helical melittin (left) and of TME (right) in the aqueous channels of the cubic phase with a series of gated fluorescence emissions.

picoseconds. The three time scales are similar for all four Trp probes, but their relative amplitudes systematically change with the probe positions in the channel. For example, at 310 nm the three components of tryptophan decay in 0.68, 8, and 80 ps with relative amplitudes of 42%, 29%, and 29%, respectively (Figure 3). For TBE, the three decay constants are similar, 1.24, 11, and 84 ps but the amplitudes change to 16%, 27%, and 57% (Figure 5). For the four Trp probes studied here, we

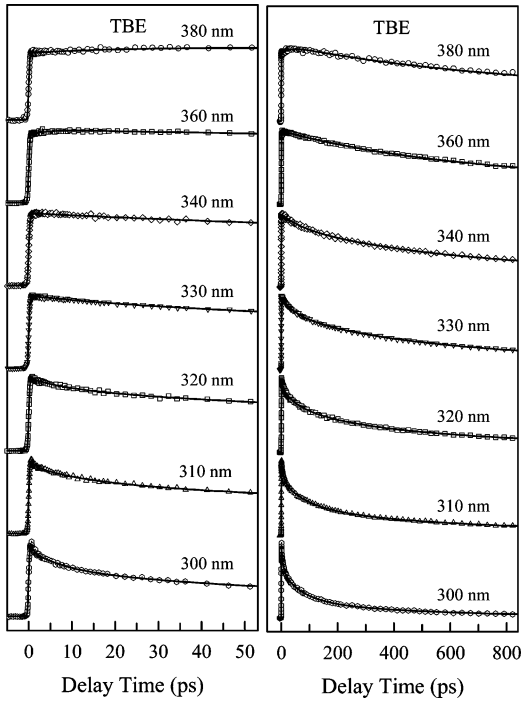

Figure 5. Normalized femtosecond-resolved fluorescence transients of TBE in the aqueous channels of the cubic phase in the short (left) and long (right) time ranges with a series of gated fluorescence emissions. Note that the solvation dynamics drastically slows down compared to the transients of tryptophan in Figure 2.

observed a correlation between their local hydrophobicity and the relative contributions of the first and third components; from Trp, to melittin, to TME, and to TBE, the first components at 310 nm have contributions of 42%, 35%, 25%, and 16%, and the third components vary from 29%, to 37%, to 40%, and to 57%, respectively. The second components have nearly constant amplitudes of approximately 30%. At the red side of the fluorescence emission, all transients show two initial rise components in the range from 0.3 to 30 ps followed by two lifetime emissions.

B. Solvation Correlation Functions. The observed decay on the blue side and rise on the red end of wavelength-gated fluorescence transients are typical signatures of solvent relaxation. The construction of the solvent response function has been well-studied using a single-lifetime dye molecule as an optical probe in solution.[37] Zhong and co-workers[12a] have demonstrated that such a conventional method is no longer applicable for the tryptophan probe because the fluorescence spectrum of excited tryptophan usually is a mixture of two emissions with two different lifetimes due to its inevitable ground-state heterogeneity. An extended method has been recently introduced to construct the solvent response function using tryptophan as a solvation probe.[12a]

Briefly, all femtosecond-resolved fluorescence transients of tryptophan can be represented as a sum of two terms of discrete exponential functions

$$I_\lambda(t) = I_\lambda^{\text{solv}}(t) + I_\lambda^{\text{popul}}(t) = \sum_i \alpha_i \, e^{-t/\tau_i} + \sum_j \beta_j \, e^{-t/\tau_j} \tag{III.1}$$

where the first term associated with α_i and τ_i describes solvation processes and the second term associated with β_j and τ_j represents intrinsic lifetime emissions (population decay). The coefficient α_i is positive (decay dynamics) at the blue side of the emission peak and is negative (initial rise) at the red side.

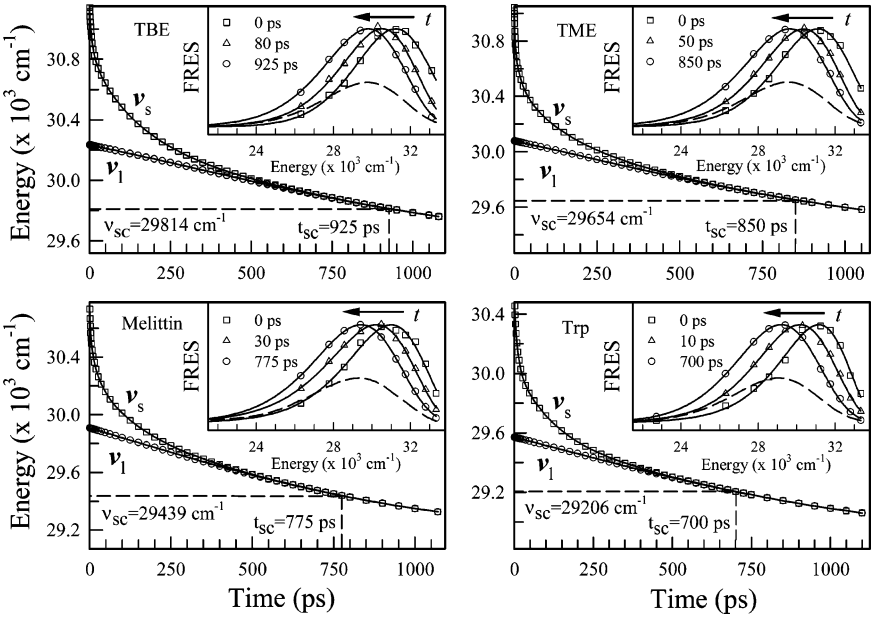

Figure 6. Femtosecond-resolved emission maxima of the overall emission spectra (ν_s) and the lifetime-associated emission spectra (ν_l) for all four Trp probes studied. In the inset is a representation of the normalized overall FRES's at several typical delay times constructed from the transients in Figures 3−5. The dashed curves are the corresponding steady-state fluorescence emission spectra.

The coefficient β_j is always positive and represents relative contributions of lifetime emissions. Thus, the *overall* time-resolved emission spectra can be constructed as follows

$$I(\lambda,t) = \frac{I_\lambda^{ss} I_\lambda(t)}{\sum_i \alpha_i \tau_i + \sum_j \beta_j \tau_j} \qquad \text{(III.2)}$$

where I_λ^{ss} is the relative steady-state emission intensity at the wavelength λ. The time-resolved spectrum, after being converted to intensity versus frequency in cm^{-1}, was fitted to a log-normal function to deduce the emission maximum $\nu_s(t)$. Thus, a function of emission maxima with time can be obtained. At a certain time (t_{sc}), solvation is complete, and the emission maximum $\nu_s(t_{sc})$ should be equal to the *apparent* lifetime emission peak $\nu_l(t_{sc})$, which results from a mixture of two lifetime emissions and is constructed from a lifetime-associated time-dependent emission spectrum

$$I^{popul}(\lambda,t) = \frac{I_\lambda^{ss} I_\lambda^{popul}(t)}{\sum_i \alpha_i \tau_i + \sum_j \beta_j \tau_j} \qquad \text{(III.3)}$$

The emission maximum $\nu_l(t)$ is also deduced from a log-normal fit of the spectrum. For convenience, we call τ_{sc} the solvation-complete time. Apparently, the emission maximum ν_{sc} at τ_{sc} differs from the steady-state emission peak ν_{ss}, and the solvation-complete time τ_{sc} is different from τ_{ss}, a time for the time-resolved spectrum to reach the steady-state emission. It is also readily realized that after solvation ends overall time-dependent emission peaks $\nu_s(t)$ merge into lifetime-associated emission maxima of $\nu_l(t)$. As a consequence of the fact that the lifetime-associated emission keeps moving to the red with time, a more accurate method is to subtract the lifetime-associated emission contribution $\nu_l(t)$ from the overall emission maximum $\nu_s(t)$, and the solvent response function can be constructed as follows

$$c(t) = \frac{\nu_s(t) - \nu_l(t)}{\nu_s(0) - \nu_l(0)} \qquad \text{(III.4)}$$

The constructed $c(t)$ function is finished at time τ_{sc}, and this correlation function can be fitted to a multiple-exponential decay. Practically, we consider the time when the difference between $\nu_s(t)$ and $\nu_l(t)$ is less than 0.5 cm^{-1} as the solvation-complete time τ_{sc}. For a molecular probe with only single-lifetime emission, $\nu_l(t) = \nu_l(0) = \nu(\infty)$ always holds because the lifetime-associated emission no longer varies with time and eq III.4 converges to the conventional one. It should be noted that the difference between $\nu_{sc}(t_{sc})$ and $\nu_{ss}(t_{ss})$ purely results from a mixture of two lifetime emissions. The steady-state emission maximum, obtained from an integration of all time-resolved spectra, is *not* relevant for the construction of a correlation function.

Using eqs III.2 and III.3, the overall femtosecond-resolved emission spectrum (FRES) was constructed, and these results are shown as an inset in Figure 6 with several typical delay times. Similarly, the FRES due to a two lifetime emission mixture was also constructed (not shown). The overall emission maxima ν_s (Stokes shifts) and lifetime-associated emission maxima ν_l, derived from the log-normal fit of the corresponding FRES, are shown in Figure 6 and summarized in Table 1. Clearly, the solvation-complete time τ_{sc} and the corresponding emission maximum ν_{sc} are quite different from τ_{ss} and ν_{ss}. For example, the water relaxation probed by tryptophan in the channel completes in 700 ps while the FRES takes 1100 ps to

TABLE 1: Emission Maxima and Time Constants from the Construction of Time-Resolved Emissions[a]

Trp probes	λ_0	λ_{sc}	τ_{sc}	λ_{ss}	τ_{ss}	λ_1	λ_2
Trp	321.00	342.40	700	344	1100	332.65	346.40
melittin	322.55	339.69	775	341	1070	328.04	343.40
TME	321.53	337.22	850	338	1050	327.21	340.54
TBE	320.23	335.41	925	336	1080	326.63	338.64

[a] All emission maxima ($\lambda = 1/\nu$) and time constants (τ) are in units of nm and ps, respectively.

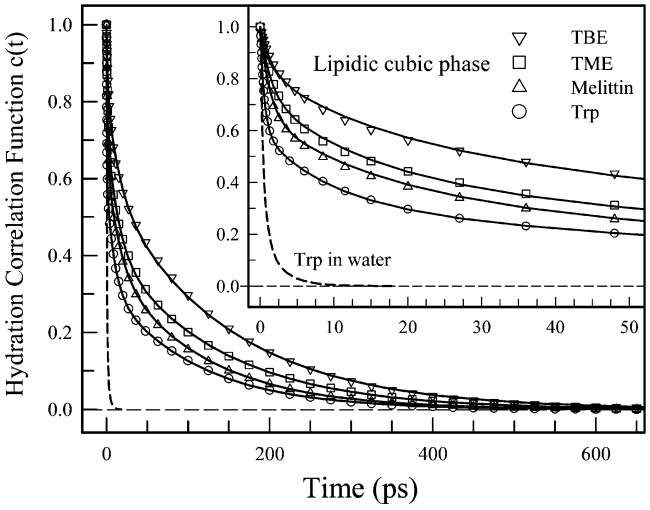

Figure 7. Hydration correlation functions obtained for four Trp probes. These functions are presented (solid line) with three distinct time scales and different relative amplitudes. The inset shows the correlation functions in the short time range. The solvation correlation function of tryptophan in bulk water is also shown (dashed line) for comparison.

TABLE 2: Results Obtained for Hydration Correlation Functions of Four Trp Probes[a]

Trp probes	τ_1	τ_2	τ_3	α_1	α_2	α_3
Trp	0.56	9.2	108	0.40	0.28	0.32
melittin	1.25	13.9	114	0.35	0.27	0.38
TME	1.38	13.7	135	0.26	0.31	0.43
TBE	1.43	15.2	147	0.17	0.30	0.53

[a] All hydration correlation functions were best fitted with $c(t) = \alpha_1 e^{-t/\tau_1} + \alpha_2 e^{-t/\tau_2} + \alpha_3 e^{-t/\tau_3}$ and $\sum_{i=1}^{3}\alpha_i = 1$. The time constants are in units of ps.

reach its steady-state emission. In the additional 400 ps, the emission further shifts 145 cm^{-1} ($\nu_{sc} - \nu_{ss}$), a process purely caused by the mixture of two lifetime emissions.

The solvation correlation functions were constructed using eq III.4, and the derived results are shown in Figure 7 and listed in Table 2. Specifically, the solvation dynamics from Trp occur in 0.56 (40%), 9.2 (28%), and 108 ps (32%). For Trp19 of melittin, the water relaxation times are 1.25 (35%), 14 (27%), and 113 ps (38%). For TME, the solvation correlation becomes 1.38 (26%), 14 (31%), and 134 ps (43%). With TBE, water motion was observed in 1.43 (17%), 15 (30%), and 147 ps (53%). Clearly, the overall solvation dynamics obtained from the four Trp probes are drastically different, indicating that the Trp probes sample different regions of channel water. However, the three time constants of water relaxation are similar, and only the corresponding amplitudes systematically change, indicating that the Trp probes sense different fractions of three types of water in the channel.

C. Hydration Dynamics and Water Structure. The observed solvation dynamics of channel water are striking. The three distinct time scales and the systematically varying amplitudes, well correlated with their hydrophobicity, strongly suggest discrete water structures in the nanochannel. These three types of water structures represent bulklike, quasi-bound, and well-ordered water distributions across the aqueous channel.

Extensive studies in reverse micelles by Levinger's group revealed a similar water distribution,[18] consistent with the distinct water model proposed by Finer.[38] For example, when the molar ratio (w_0) of water to surfactant is 6.8 in lecithin reverse micelles with a corresponding diameter of ~37 Å, three solvation time scales of 0.57 (13%), 14 (25%), and 320 ps (62%) were observed using coumarin 343 as the molecular probe. At $w_0 = 4.8$ with a ~30 Å water core diameter, only a single solvation dynamic was observed at 217 ps, indicating that all water molecules are well-ordered inside the aqueous pool. The lecithin in these reverse micelles have charged headgroups, which have much stronger interactions with water than the neutral headgroups of monoolein in the cubic phase channels. The longest solvation component (~200−300 ps) represents water relaxation near the charged headgroups at the lecithin interface and is expected to be slower than that of monoolein interfacial channel water (~100 ps). In the latter case, the channel diameter is approximately 50 Å and is equivalent to $w_0 \approx 11.4$ in reverse micelles. Thus, there is considerable free bulk water at the core of the nanochannel.

The response range of the local environment to the excited Trp probe is mainly within 7−10 Å because the dipole−dipole interaction at 7−10 Å to that at ~3.5 Å of the first solvent shell drops to 12.5−4.3%. This interaction distance is also confirmed by recent calculations.[39] Thus, the hydration dynamics that we obtained from each Trp probe reflects water motion in the approximately three neighboring solvent shell. There are approximately seven layers of water molecules in the 50 Å channel, and we observed three discrete dynamic structures. We estimated approximately four layers of bulklike free water near the channel center, approximately two layers of quasi-bound water networks in the middle, and one layer of well-ordered rigid water at the lipid interface. Because of lipid fluctuation, water can penetrate into the lipid headgroups, and one more trapped water layer is probably buried in the headgroups. As a result, about two bound water layers exist around the lipid interface. The obtained distribution of distinct water structures is also consistent with ~15 Å of hydration observed by X-ray diffraction studies from White's group.[40] These discrete water structures in the nanochannel are schematically shown in Figure 8, and these water molecules are all in dynamic equilibrium.

The tryptophan butyl ester and octyl ester in the cubic phase give the same fluorescence emission maximum at 336 nm, indicating that both TBE and TOE insert into the lipid headgroups (Figure 1) but are not buried in the lipid hydrocarbon chains because tryptophan in a truly hydrophobic environment has an emission maximum at less than 330 nm. Also, TBE is not located at the lipid surface because surface tryptophan has a maximum close to ~340 nm. We also measured the anisotropic dynamics, and the result (Figure 9) is consistent with highly restricted wobbling motions by lipid headgroups with a long decay time constant of 726 ps. TBE in water takes less than 100 ps to complete rotational relaxation. More importantly, the anisotropy finally stays at a constant within 1.5 ns after partial orientational relaxation, showing that TBE experiences a hindered local motion by the lipid headgroups. Recent experiments and molecular dynamics (MD) simulations[41] in micelles also supported the insertion position of TOE into the headgroups. Thus, the observed 147 ps solvation dynamics mainly results from the trapped and ordered water motion around the lipid interface. The contribution from the headgroups would be minor.[33] The 15 ps hydration relaxation reflects the quasi-bound water motion near the lipid interface, and this time scale is very similar to that of the surface water motion of proteins. The ultrafast component in 1.43 ps can be from bulklike water relaxation as well as the initial libration of ordered water molecules. According to the location of TBE in the channel (position 1 in Figure 8) and the sensitivity of the Trp probe, the observed ultrafast dynamics favors the latter contribution

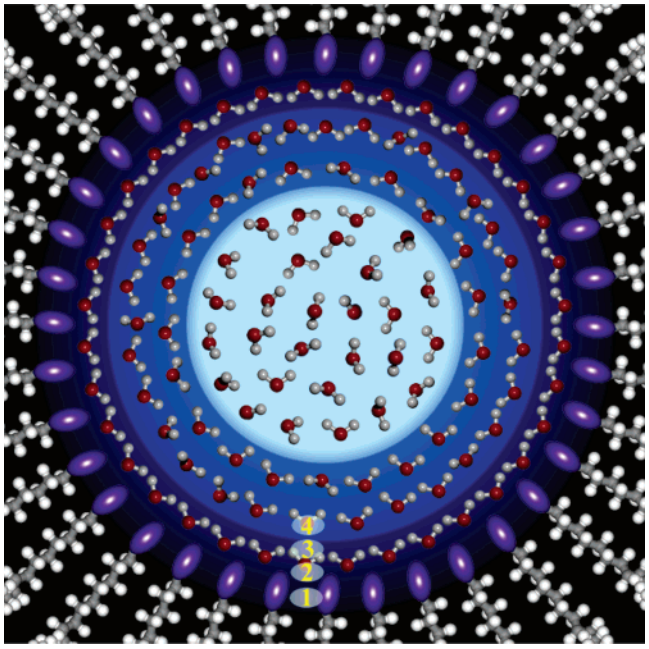

Figure 8. Schematic representation of water structure in aqueous nanochannels ~50 Å in diameter. By anchoring four Trp probes into lipid bilayers, these molecular rulers measure water motions in different local regions in the channel as shown in positions 1−4 of TBE, TME, melittin, and Trp. The Trp probe senses an interaction range with its local environment in a diameter of ~7−10 Å. A layer of trapped water buried in the lipid headgroup region is not shown. The blue represents different layers of water structures.

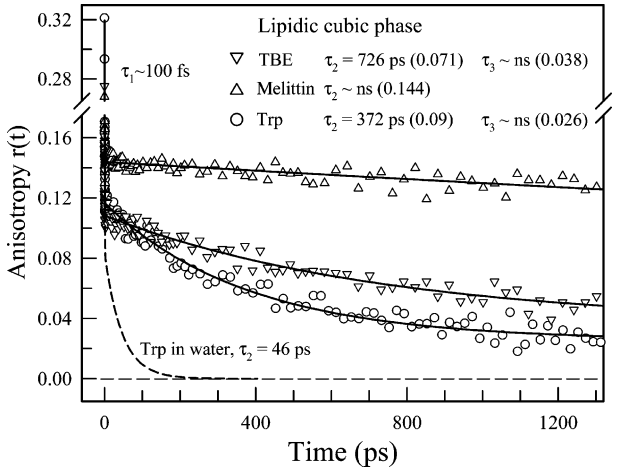

Figure 9. Time-resolved fluorescence anisotropy decays of Trp probes in the aqueous channels of the cubic phase. The initial ~100 fs decay results form the ultrafast internal conversion between ^1L_a and ^1L_b. For clarity, the anisotropy of TME is not shown, and its orientational relaxation takes 440 ps between Trp (372 ps) and TBE (726 ps). The relaxation of Trp in bulk water (46 ps) is also shown (dashed line) for comparison. Note that all observed rotational time constants are significantly longer than the relaxation of Trp in bulk water.

of libration. The overall orientation of well-ordered water at the lipid interface, although in a fluctuation on the time scale of ~150 ps, aligns along the lipid headgroup polarization, resulting in its dipole direction pointing to the channel center (Figure 8), as is confirmed by recent MD simulations.[42]

With the probe position moving toward the center of the aqueous channel, we detected more ultrafast and fewer slow solvation components. Note the negligible change of the quasi-bound water contributions, indicating the complete detection of the two layers of quasi-bound water by all four Trp probes. For TME, the fluorescence emission peak shifts to 338 nm, and its location moves to the lipid interface (Figure 8). We did observe a smaller fraction of slow solvation dynamics decreasing from 53% in TBE to 43% in TME and an increase of the ultrafast component from 17% to 26%. The corresponding anisotropy dynamics drops from 726 to 440 ps with a less hindered local motion at the lipid interface.

The emission of Trp19 in melittin further shifts to the red peaking at 341 nm (Figure 2), and the probe location slightly moves away from the lipid interface toward the channel center. Consistently, we observed a larger fraction of the ultrafast solvation component (35%) and a smaller contribution of the slow ordered water motion (38%). Melittin consists of 26 amino acid residues (G-I-G-A-V-L-K-V-L-T-T-G-L-P-A-L-I-S-**W**-I-K-R-K-R-Q-Q), and the first 20 residues are predominantly hydrophobic while the other six near the carboxyl terminus are hydrophilic under physiological conditions. This amphipathic property makes melittin easily bound to membranes and extensive studies from both experiments,[34,43−45] and MD simulations[46−48] have shown the formation of an α-helix at the lipid interface. Self-assembly of α-helical melittin monomers is believed to be important in its lytic activity of membranes.[34] Our observed hydration dynamics are consistent with previous studies, supporting the view that melittin forms an α-helix and inserts into the lipid bilayers, leaving the hydrophilic C-terminus protruding into the water channel. The orientational relaxation shows completely restricted motion of Trp19, and the anisotropy is constant in 1.5 ns (Figure 9), consistent with Trp19 located close to the interface around the headgroups and rigid well-ordered water molecules.

Tryptophan emission in the channel shifts another 3 nm to the red and peaks at 344 nm (Figure 2) while it has a maximum at ~350 nm in bulk water. Thus, the probe location moves toward the channel center, but it is situated in the quasi-bound water layer (Figure 8), consistent with the obtained hydration results. Again, we observed an increase in the ultrafast component (40%) and a decrease of the slow contribution (32%). The observed 108 ps slow dynamics are still from the ordered water motion at the interface and the 9.2 ps component from the quasi-bound water relaxation. The 0.56 ps dynamics represents ultrafast bulklike water motion and local libration,[49,50] indicating that a significant fraction of bulklike water (≤40%) was probed. The femtosecond-resolved anisotropy showed a local restricted motion with a relaxation time of 372 ps (Figure 9), one order of magnitude slower than that in bulk water (46 ps), revealing local rigid water networks and consistent with aforementioned hydration results.

IV. Conclusion

In this article, we reported on systematic studies of hydration dynamics in the water nanochannels of the lipidic cubic phase with a series of Trp−alkyl ester probes. By anchoring the hydrocarbon tails at different depths in the lipid bilayer, we mapped out with femtosecond resolution the entire profile of water motions across the nanochannel. Three distinct time scales were observed, revealing three discrete water structures in the channel. Approximately two layers of well-ordered interfacial water are bound to the lipid headgroups, and the relaxation dynamics occurs in ~100−150 ps. These dynamically rigid water molecules are crucial for global structural stability and local conformational flexibility of lipid bilayers.[51] The adjacent two layers near the lipid interface are hydrogen-bonded water networks in which dynamic relaxation takes place in 10−15 ps, one order of magnitude faster than the confined interfacial

water. This quasi-bound water motion is similar to typical protein surface hydration relaxation.[11,12,52,53] The water near the channel center is bulklike, and the dynamics take less than 1 ps. The corresponding anisotropy relaxation in different locations is well correlated with the hydration dynamics and local water rigidity.

The observed discrete water dynamics and structures in the nanochannel are significant and probably impact on the nanoscopic interactions of biomolecules with water and lipids. The ultrafast bulklike water motion in less than 1 ps freely transports biomolecules near the channel center, consistent with the related transport studies.[32b,c] The well-ordered water at the lipid interface facilitates anchoring of biomolecules in the lipid bilayer with dynamical rigidity on the time scale of hundreds of picoseconds. The quasi-bound water near the lipid interface fluctuates in tens of picoseconds and maintains biomolecular conformational flexibility for biological function. Water is unique in nanoconfinements and can adopt various structures and dynamic motions for performing different biological functions and having exceptional properties of nanomaterials.

Acknowledgment. The authors thank K. Reidl, J. Clogston, and W. Liu for technical assistance. Supported in part by grants from the ACS Petroleum Research Fund (PRF42734-G4) and the National Science Foundation (CHE-0517334) and the Packard Fellowship to D.Z. and grants from Science Foundation Ireland (02-IN1-B266) and the National Institutes of Health (GM61070 and GM075915) to M.C.

References and Notes

(1) (a) Pal, S. K.; Zewail, A. H. *Chem. Rev.* **2004**, *104*, 2099. (b) Pal, S. K.; Peon, J.; Bagchi, B.; Zewail, A. H. *J. Phys. Chem. B* **2002**, *106*, 12376.

(2) Levinger, N. E. *Science* **2002**, *298*, 1722.

(3) Mattos, C. *Trends Biochem. Sci.* **2002**, *27*, 203.

(4) Nandi, N.; Bhattacharyya, K.; Bagchi, B. *Chem. Rev.* **2000**, *100*, 2013.

(5) (a) Koga, K.; Gao, G. T.; Tanaka, H.; Zeng, X. C. *Nature* **2001**, *412*, 802. (b) Koga, K.; Tanaka, H.; Zeng, X. C. *Nature* **2000**, *408*, 564.

(6) (a) Fitter, J.; Lechner, R. E.; Dencher, N. A. *J. Phys. Chem. B* **1999**, *103*, 8036. (b) Gelbart, W. M.; Ben-Shaul, A. *J. Phys. Chem.* **1996**, *100*, 13169.

(7) (a) Finney, J. L. *Faraday Discuss.* **1996**, *103*, 1 and references therein. (b) *Protein*−*Solvent Interactions*; Gregory, R. B., Ed.; Marcel Dekker: New York, 1995.

(8) (a) Jurkiewicz, P.; Sykora, J.; Olzynska, A.; Humpolickova, J.; Hof, M. *J. Fluoresc.* **2005**, *15*, 883. (b) Chattopadhyay, A.; Arora, A.; Kelkar, D. A. *Eur. Biophys. J.* **2005**, *35*, 62.

(9) Bhide, S. Y.; Berkowitz, M. L. *J. Chem. Phys.* **2005**, *123*, 224702.

(10) de Gennes, P. G. *Rev. Mod. Phys.* **1992**, *64*, 645.

(11) (a) Pal, S. K.; Peon, J.; Zewail, A. H. *Proc. Natl. Acad. Sci. U.S.A.* **2002**, *99*, 1763. (b) Peon, J.; Pal, S. K.; Zewail, A. H. *Proc. Natl. Acad. Sci. U.S.A.* **2002**, *99*, 10964. (c) Zhao, L.; Pal, S. K.; Xia, T.; Zewail, A. H. *Angew. Chem., Int. Ed.* **2004**, *43*, 60.

(12) (a) Lu, W.; Kim, J.; Qiu, W.; Zhong, D. *Chem. Phys. Lett.* **2004**, *388*, 120. (b) Lu, W.; Qiu, W.; Kim, J.; Okobiah, O.; Hu, J.; Gokel, G. W.; Zhong, D. *Chem. Phys. Lett.* **2004**, *394*, 415. (c) Qiu, W.; Zhang, L.; Kao, Y. -T.; Lu, W.; Li, T.; Kim, J.; Sollenberger, G. M.; Wang, L.; Zhong, D. *J. Phys. Chem. B* **2005**, *109*, 16901. (d) Qiu, W.; Zhang, L.; Okobiah, O.; Yang, Y.; Wang, L.; Zhong, D.; Zewail, A. H. *J. Phys. Chem. B* **2006**, *110*, 10540.

(13) Kong, Y.; Ma, J. *Proc. Natl. Acad. Sci. U.S.A.* **2001**, *98*, 14345.

(14) Pomes, R.; Roux, B. *Biophys. J.* **2002**, *82*, 2304.

(15) (a) Lanyi, J. K. *J. Phys. Chem. B* **2000**, *104*, 11441. (b) Garczarek, F.; Gerwert, K. *Nature* **2006**, *439*, 109.

(16) (a) Brauns, E. B.; Madaras, M. L.; Coleman, R. S.; Murphy, C. J.; Berg, M. A. *J. Am. Chem. Soc.* **1999**, *121*, 11644. (b) Brauns, E. B.; Madaras, M. L.; Coleman, R. S.; Murphy, C. J.; Berg, M. A. *Phys. Rev. Lett.* **2002**, *88*, 158101.

(17) (a) Pal, S. K.; Zhao, L.; Zewail, A. H. *Proc. Natl. Acad. Sci. U.S.A.* **2003**, *100*, 8113. (b) Pal, S. K.; Zhao, L.; Xia, T.; Zewail, A. H. *Proc. Natl. Acad. Sci. U.S.A.* **2003**, *100*, 13746.

(18) (a) Harpham, M. R.; Ladanyi, B. M.; Levinger, N. E.; Herwig, K. W. *J. Chem. Phys.* **2004**, *121*, 7855. (b) Willard, D. M.; Riter, R. E.; Levinger, N. E. *J. Am. Chem. Soc.* **1998**, *120*, 4151. (c) Riter, R. E.; Willard, D. M.; Levinger, N. E. *J. Phys. Chem. B* **1998**, *102*, 2705. (d) Pant, D.; Riter, R. E.; Levinger, N. E. *J. Chem. Phys.* **1998**, *109*, 9995.

(19) (a) Bhattacharyya, K.; Bagchi, B. *J. Phys. Chem. A* **2000**, *104*, 10603. (b) Bhattacharyya, K. *Acc. Chem. Res.* **2003**, *36*, 95.

(20) (a) Piletic, I. R.; Tan, H. S.; Fayer, M. D. *J. Phys. Chem. B* **2005**, *109*, 21273. (b) Tan, H. S.; Piletic, I. R.; Riter, R. E.; Levinger, N. E.; Fayer, M. D. *Phys. Rev. Lett.* **2005**, *94*, 057405. (c) Tan, H. S.; Piletic, I. R.; Fayer, M. D. *J. Chem. Phys.* **2005**, *122*, 174501.

(21) (a) Pant, D.; Levinger, N. E. *Chem. Phys. Lett.* **1998**, *292*, 200. (b) Pant, D.; Levinger, N. E. *J. Phys. Chem. B* **1999**, *103*, 7846.

(22) Maniwa, Y.; Kataura, H.; Abe, M.; Suzuki, S.; Achiba, Y.; Kira, H.; Matsuda, K. *J. Phys. Soc. Jpn.* **2002**, *71*, 2863.

(23) Cheng, J.; Pautot, S.; Weitz, D. A.; Xie, X. S. *Proc. Natl. Acad. Sci. U.S.A.* **2003**, *100*, 9826.

(24) (a) Temsamani, M. B.; Maeck, M.; El Hassani, I.; Hurwitz, H. D. *J. Phys. Chem. B* **1998**, *102*, 3335. (b) Venables, D. S.; Huang, K.; Schmuttenmaer, C. A. *J. Phys. Chem. B* **2001**, *105*, 9132.

(25) Mittleman, D. M.; Nuss, M. C.; Colvin, V. L. *Chem. Phys. Lett.* **1997**, *275*, 332.

(26) (a) Hauser, H.; Haering, G.; Pande, A.; Luisi, P. L. *J. Phys. Chem.* **1989**, *93*, 7869. (b) D'Aprano, A.; Lizzio, A.; Liveri, V. T.; Aliotta, F.; Vasi, C.; Migliardo, P. *J. Phys. Chem.* **1988**, *92*, 4436.

(27) Shirota, H.; Horie, K. *J. Phys. Chem. B* **1999**, *103*, 1437.

(28) Kolesnikov, A. I.; Zanotti, J.; Loong, C. K.; Thiyagarajan, P. *Phys. Rev. Lett.* **2004**, *93*, 035503.

(29) (a) Landau, E. M.; Rosenbusch, J. P. *Proc. Natl. Acad. Sci. U.S.A.* **1996**, *93*, 14532. (b) Rummel, G.; Hardmeyer, A.; Widmer, C.; Chiu, M. L.; Nollert, P.; Locher, K. P.; Pedruzzi, I.; Landau, E. M.; Rosenbusch, J. P. *J. Struct. Biol.* **1998**, *121*, 82.

(30) (a) Caffrey, M. *Curr. Opin. Struct. Biol.* **2000**, *10*, 486. (b) Caffrey, M. **2002**, *12*, 471. (c) Caffrey, M. *J. Struct. Biol.* **2003**, *142*, 108.

(31) (a) Luecke, H.; Schobert, B.; Lanyi, J. K.; Spudich, E. N.; Spudich, J. L. *Science* **2001**, *293* 1499. (b) Gordeliy, V. I.; Labahn, J.; Moukhametzianov, R.; Efremov, R.; Granzin, J.; Schlesinger, R.; Buldt, G.; Savopol, T.; Scheidig, A. J.; Klare, J. P.; Engelhard, M. *Nature* **2002**, *419*, 484.

(32) (a) Raman, P.; Cherezov, V.; Caffrey, M. The Membrane Protein Data Bank. *Cell. Mol. Life Sci.* **2006**, *63*, 36. http://www.mpdb.ul.ie/. (b) Clogston, J.; Craciun, G.; Hart, D. J.; Caffrey, M. *J. Controlled Release* **2005**, *102*, 441. (c) Clogston, J.; Caffrey, M. *J. Controlled Release* **2005**, *107*, 97. (d) Liu, W.; Caffrey, M. *Biochemistry* **2006**, *45*, 11713.

(33) (a) Faeder, J.; Ladanyi, B. M. *J. Phys. Chem. B* **2000**, *104*, 1033. (b) Faeder, J.; Ladanyi, B. M. **2001**, *105*, 11148. (c) Faeder, J.; Ladanyi, B. M. **2005**, *109*, 6732.

(34) (a) Ohki, S.; Marcus, E.; Sukumaran, D. K.; Arnold, K. *Biochim. Biophys. Acta* **1994**, *1194*, 223. (b) Frey, S.; Tamm, L. K. *Biophys. J.* **1991**, *60*, 922. (c) Dempsey, C. E. *Biochim. Biophys. Acta* **1990**, *1031*, 143.

(35) Saxena, C.; Sancar, A.; Zhong, D. *J. Phys. Chem. B* **2004**, *108*, 18026.

(36) Cherezov, V.; Clogston, J.; Misquitta, Y.; Abdel-Gawad, W.; Caffrey, M. *Biophys. J.* **2002**, *83*, 3393.

(37) (a) Maroncelli, M.; Fleming, G. R. *J. Chem. Phys.* **1987**, *86*, 6221. (b) Horng, M. L.; Gardecki, J.; Papazyan, A.; Maroncelli, M. *J. Phys. Chem.* **1995**, *99*, 17311.

(38) Finer, E. G. *J. Chem. Soc., Faraday Trans. 2* **1973**, *69*, 1590.

(39) Vivian, J. T.; Callis, P. R. *Biophys. J.* **2001**, *80*, 2093.

(40) (a) Hristova, K.; White, S. H. *Biophys. J.* **1998**, *74*, 2419. (b) Wiener, M. C.; White, S. H. *Biophys. J.* **1992**, *61*, 434.

(41) de Foresta, B.; Gallay, J.; Sopkova, J.; Champeil, P.; Vincent, M. *Biophys. J.* **1999**, *77*, 3071.

(42) Wilson, M. A.; Pohorille, A. *J. Am. Chem. Soc.* **1994**, *116*, 1490.

(43) (a) Raghuraman, H.; Chattopadhyay, A. *Biophys. J.* **2004**, *87*, 2419. (b) Raghuraman, H.; Chattopadhyay, A. *Langmuir* **2003**, *19*, 10332. (c) Chattopadhyay, A.; Rukmini, R. *FEBS Lett.* **1993**, *335*, 341.

(44) Ladokhin, A. S.; Jayasinghe, S.; White, S. H. *Anal. Biochem.* **2000**, *285*, 235.

(45) (a) Tran, C. D.; Beddard, G. S. *Eur. J. Biophys.* **1985**, *13*, 59. (b) John, E.; Jahnig, F. *Biophys. J.* **1988**, *54*, 817.

(46) Roccatano, D.; Colombo, G.; Fioroni, M.; Mark, A. E. *Proc. Natl. Acad. Sci. U.S.A.* **2002**, *99*, 12179.

(47) (a) Lin, J. H.; Baumgaertner, A. *Biophys. J.* **2000**, *78*, 1714. (b) Bachar, M.; Becker, O. M. *J. Chem. Phys.* **1999**, *111*, 8672.

(48) (a) Cheng, Y. K.; Rossky, P. J. *Nature* **1998**, *392*, 696. (b) Cheng, Y. K.; Sheu, W. S.; Rossky, P. J. *Biophys. J.* **1999**, *76*, 1734.

(49) Zhong, D.; Pal, S. K.; Zhang, D.; Chan, S. I.; Zewail, A. H. *Proc. Natl. Acad. Sci. U.S.A.* **2002**, *99*, 13.

(50) Shen, X. H.; Knutson, J. R. *J. Phys. Chem. B* **2001**, *105*, 6260.

(51) Lee, A. G. *Biochim. Biophys. Acta* **2003**, *1612*, 1.

(52) Kao, Y. -T.; Zhong, D., to be submitted for publication.

(53) Bizzarri, A. R.; Cannistraro, S. *J. Phys. Chem. B* **2002**, *106*, 6617.